HHS Public Access

Author manuscript

Immunohorizons. Author manuscript; available in PMC 2023 May 26.

Published in final edited form as:

Immunohorizons. ; 6(2): 156–169. doi:10.4049/immunohorizons.2200011.

FLAMs: A self-replicating *ex vivo* model of alveolar macrophages for functional genetic studies

Sean Thomas[1,*], **Kathryn Wierenga**[2,3,*], **James Pestka**[3,4,5], **Andrew J Olive**[1]

[1]Department of Microbiology and Molecular Genetics, College of Osteopathic Medicine, Michigan State University, East Lansing MI USA.

[2]Department of Biochemistry and Molecular Biology, Michigan State University, East Lansing, MI 48824, U.S.

[3]Institute for Integrative Toxicology, Michigan State University, East Lansing, MI 48824, U.S.

[4]Department of Microbiology and Molecular Genetics, Michigan State University, East Lansing, MI 48824, U.S.

[5]Department of Food Science and Human Nutrition, East Lansing, MI 48824, U.S.

Abstract

Alveolar macrophages (AMs) are tissue resident cells in the lungs derived from the fetal liver that maintain lung homeostasis and respond to inhaled stimuli. While the importance of AMs is undisputed, they remain refractory to standard experimental approaches and high-throughput functional genetics as they are challenging to isolate and rapidly lose AM properties in standard culture. This limitation hinders our understanding of key regulatory mechanisms that control AM maintenance and function. Here, we describe the development of a new model, fetal liver-derived alveolar-like macrophages (FLAMs), which maintains cellular morphologies, expression profiles, and functional mechanisms similar to murine AMs. FLAMs combine treatment with two key cytokines for AM maintenance, GM-CSF and TGFβ. We leveraged the long-term stability of FLAMs to develop functional genetic tools using CRISPR-Cas9-mediated gene editing. Targeted editing confirmed the role of AM-specific gene *Marco* and the IL-1 receptor *Il1r1* in modulating the AM response to crystalline silica. Furthermore, a genome-wide knockout library using FLAMs identified novel genes required for surface expression of the AM marker Siglec-F, most notably those related to the peroxisome. Taken together, our results suggest that FLAMs are a stable, self-replicating model of AM function that enables previously impossible global genetic approaches to define the underlying mechanisms of AM maintenance and function.

Keywords

Macrophage; lung; silica; CRISPR; TGFβ; Siglec-F; IL-1; MARCO; peroxisomes

Corresponding Author: Andrew Olive Ph.D., Department of Microbiology and Molecular Genetics, College of Osteopathic Medicine, Michigan State University, East Lansing, MI 48824, U.S., oliveand@msu.edu.

*These authors contributed equally to this work.

Competing Interests

The authors have no competing interests related to the research described in this manuscript.

INTRODUCTION

Tissue resident immune cells regulate homeostasis and control local inflammation to external stimuli. A subset of these immune cells are tissue resident macrophages (TRMs) that sample the environment and initiate host responses (1). Distinct TRM populations exist in specific tissues including the liver (Kupffer cells), the skin (Langerhans cells), the brain (microglia), and the lungs (alveolar macrophages [AMs]). These distinct TRMs all have unique functions that are regulated by the local environment and are required for tissue maintenance (2, 3).

As the first line of defense in the airways, AMs are particularly important for tuning the host immune response in the lungs (4). AMs can be distinguished from other macrophage populations in the lung by the surface expression of the sialic acid receptor Siglec-F, the scavenger receptor MARCO, and the integrin CD11c in addition to the high expression and activity of the transcription factor PPARγ, which drives many AM-specific genes (5, 6). AMs are a long-lived and self-replicating and, like most TRMs, are derived from embryonic precursors (7). AMs arise from fetal liver monocytes, which migrate to the lung and develop into mature AMs in the presence of cytokines such as GM-CSF and TGFβ shortly after birth (8–10). The continued presence of these factors is necessary for the maintenance and self-renewal of AMs in the lung, in part by promoting expression and activation of PPARγ (10, 11). Genes and pathways induced by this receptor are involved in lipid metabolism and induction of scavenger receptors that promote phagocytosis (12). This is critical for the AM roles of maintaining surfactant homeostasis, efferocytosis of cellular debris, and phagocytosis of inhaled microbes and particles in the alveolar space (12, 13). Impaired clearance of surfactant by AMs can result in the pathophysiological condition known as pulmonary alveolar proteinosis (PAP) (14). In addition, reduced AM efferocytosis and phagocytosis has been observed in patients with asthma, COPD, and cystic fibrosis, likely contributing to the sustained inflammation and susceptibility to infection observed in these diseases (15–19).

Despite the paramount importance of AMs for lung health, there continue to be key gaps in our understanding of how they are maintained and function to regulate the host response in the lungs. One hurdle towards a mechanistic understanding of AMs is that experiments employing primary AMs require large numbers of animals to isolate a small number of cells that do not robustly proliferate or maintain AM-like functions *ex vivo* (20). This limitation has prevented genetic approaches from being employed to better understand AM maintenance and function. As a result, many *ex vivo* studies investigating responses to airborne particles and microbes rely on bone-marrow derived macrophages (BMDMs) or transformed macrophage cell lines as surrogates of AM biology (21–23). While these macrophage models are useful, they do not faithfully recapitulate all AM functions (24–26). A recent alternative approach cultured cells from the murine fetal liver in the presence of GM-CSF to generate AM-like cells that are functionally and phenotypically like AMs (25). This approach enabled the isolation of large numbers of AM-like cells that might be amenable to tractable genetic approaches. However, we found here that fetal liver-derived cells cultured in GM-CSF alone lost their AM-like morphology, phenotype, and surface marker expression over time, suggesting that GM-CSF is insufficient to maintain the AM-

like phenotype. A recent study found that AMs could be continuously cultured *ex vivo* in the presence of GM-CSF and TGFβ (27), which is consistent with reports that TGFβ promotes AM development and maintains AM function both *in vivo* and *ex vivo* (10).

Here, we found that growing fetal liver cells in both GM-CSF and TGFβ results in a long-term stable population of cells that are phenotypically and functionally similar to AMs. Using these fetal liver-derived alveolar-like macrophages (FLAMs), we developed targeted and global genetic tools to dissect regulatory networks that are required to maintain AM-like cells and function. Employing targeted gene-editing, we show here that directed mutations are readily introduced in FLAMs to query specific AM functions. We further demonstrate the utility of FLAMs by using genome-wide CRISPR-Cas9 knockout screen to identify genes that are required for the surface expression of the AM-specific marker Siglec-F. The screen identified key pathways used to maintain Siglec-F expression and the AM-like state including the observation that peroxisome biogenesis plays a central role in maintaining AM functions. Together our results show that FLAMs enable the global dissection of AM regulatory mechanisms at a previously impossible scale.

MATERIALS AND METHODS

Oligos Used in Study

Gene Target	Pair Number	Directionality	Sequence
MARCO	1	F	CACCGTTCCAGATTAAAGGTGAACG
MARCO	1	R	AAACCGTTCACCTTTAATCTGGAAC
MARCO	2	F	CACCGTAGGTCTCACTGGCCCCAAG
MARCO	2	R	AAACCTTGGGGCCAGTGAGACCTAC
MARCO	3	F	CACCGCAATGGATCACTAGCTATCG
MARCO	3	R	AAACCGATAGCTAGTGATCCATTGC
SiglecF	1	F	CACCGAAGGTCGATTCTATCTCATG
SiglecF	1	R	AAACCATGAGATAGAATCGACCTTC
SiglecF	2	F	CACCGAGCATCTCTGCAGATCCAAG
SiglecF	2	R	AAACCTTGGATCTGCAGAGATGCTC
SiglecF	3	F	CACCGCATCCAAGTCACATCTACCC
SiglecF	3	R	AAACGGGTAGATGTGACTTGGATGC
IL1R1	1	F	CACCGCAGCAAGACCCCCATATCAG
IL1R1	1	R	AAACCTGATATGGGGGTCTTGCTGC
IL1R1	2	F	CACCGCGTATGTCCTATACGTTCCG
IL1R1	2	R	AAACCGGAACGTATAGGACATACGC
IL1R1	3	F	CACCGACTGTGTTAGAGAATGACCC
IL1R1	3	R	AAACGGGTCATTCTCTAACACAGTC

Animals

Experimental protocols were approved by the Institutional Animal Care and Use Committee at MSU (AUF # PROTO201800113). 6–8 week old C57Bl6 mice (cat # 000664) and $Cas9^{+}$ mice (cat # 026179) were obtained from Jackson Laboratories (Bar Harbor, ME). Mice

were given free access to food and water under controlled conditions (humidity: 40–55%; lighting: 12 hour light/dark cycles; and temperature: 24±2°C) as described previously (28, 29). Pregnant dams at 8–10 weeks of age and 14–18 gestational days were euthanized to obtain murine fetuses. AMs were isolated from male and female mice older than 10 weeks of age. BMDMs were obtained from male and female mice 6 weeks of age and older.

FLAMs cell isolation and culture

Fetal liver derived cells were obtained as previously described (30). Briefly, pregnant dams were euthanized by CO_2 inhalation for 10 min to ensure death to neonates, which are resistant to anoxia. Cervical dislocation was used as a secondary form of death for the dam. Fetuses were immediately removed, and loss of maternal blood supply served as a secondary form of death for the fetuses. Cells were cultured in complete Roswell Park Memorial Institute medium (RPMI, Thermo Fisher) containing 10% fetal bovine serum (FBS, R&D Systems), 1% penicillin-streptomycin (P/S, Thermo Fisher), 30 ng/mL recombinant mGM-CSF (Peprotech), and 20 ng/mL recombinant hTGFβ1 (Peprotech) included where indicated. Media was refreshed every 2–3 days. When cells reached 70–90% confluency, they were lifted by incubating for 10 minutes with 37°C phosphate-buffered saline (PBS) containing 10 mM EDTA, followed by gentle scraping. After approximately 1 week, adherent cells adopted a round, AM-like morphology. At this time, stocks were frozen for future use. Thawed stocks were plated in untreated Petri dishes with either GM-CSF or GM-CSF and TGFβ (20 ng/mL recombinant hTGFβ1 [Peprotech]) and sub-cultured as described above.

AM isolation and culture

Mice were euthanized by CO_2 exposure followed by exsanguination via the inferior vena cava. Lungs were lavaged as previously described (20). Cells were then resuspended in RPMI media containing 30 ng/mL GM-CSF and plated in untreated 48- or 24- well plates. AMs were lifted from plates using Accutase™ (BioLegend) and seeded for experiments.

BMDM isolation and culture

C57BL/6J mice were euthanized by CO_2 exposure followed by cervical dislocation. Both femurs were cut on one end to expose the bone marrow, placed cut side down in 0.6 mL tubes, and centrifuged at 16,000 ×g for 25 seconds. Marrow from multiple mice was pooled, dissociated to a single cells suspension in sterile PBS and pelleted by centrifuging at 220 ×g for 5 min. The pellet was resuspended in mouse RBC lysis buffer (Alfa Aeser) and incubated at room temperature for 5 minutes. The RBC lysis buffer was diluted with 2 volumes of PBS and the cell suspension passed through a nylon 70 μm filter (Corning). Cells were pelleted a second time and resuspended in RPMI media containing 10% FBS, 1% P/S, and 20% L929 media (31). Approximately 5×10^6 cells were plated per dish in 10 cm untreated petri dishes. Media was refreshed every 2–3 days. Cells were used for assays when fully differentiated after 7 days.

Flow cytometry

Plated cells were lifted in warm PBS with 10 mM EDTA for 5–10 minutes and washed twice in PBS before fluorescent antibody labeling. Immediately following isolation, AMs were resuspended in PBS and filtered through a 70 μm basket filter and incubated with an antibody cocktail of PE CD170, APC CD11c, APC-Cyanine7 CD14, and FC Block (Biolegend; 1:400 in PBS) for 20 min at room temperature in light-free condition. Immunochemically labeled cells were washed three times with PBS, resuspended in PBS, and passed through a 70 μm nylon filter immediately prior to analysis. Flow cytometry was performed on a LSR II Flow Cytometer (BD Biosciences) at the Michigan State University Flow Cytometry Core.

qPCR

RNA was isolated from ~5×10^5 cells using RNeasy mini kits (Qiagen), typically yielding 100–400 ng RNA. RNA was then reverse transcribed to cDNA using a High-Capacity cDNA reverse transcription kit (Thermo Fisher) on a Stratagene Robocycler 40. Quantitative real-time qPCR was performed using specific Taqman probes (Thermo Fisher) for TGFβ1 (*Tgfb1*), TGFβ receptors (*Tgfbr1, Tgrbr1*), selected genes used to distinguish AMs from other macrophage populations (*Cd14, Siglecf, Marco, Pparg Car4, Fabp4, Itgax*), and cytokines *(Il1a, Il1b, Il10*) on an Applied Biosystems™ QuantStudio™ 7 real-time PCR system. Data were analyzed with Applied Biosystems™ Thermo Fisher Cloud using the RQ software and the relative quantification method. *Gapdh* was used as the housekeeping gene. Relative copy number (RCN) for each gene was normalized to expression of *Gapdh* and calculated as described previously (32).

Scanning electron microscopy

Suspensions of AMs or FLAMs were diluted to 2.5×10^5 cells/mL, and 100 μL pipetted directly upon glass 12 mm diameter, 0.13–0.16 mm thick circular coverslips (Electron Microscopy Sciences), which were placed in the bottom of 6-well plates. Cells were allowed to settle for 2–3 minutes, then 1 mL of media was added to fill the well. To fix cells, the coverslips were removed from the wells, submerged in 4% glutaraldehyde in 0.1 M sodium phosphate buffer at pH 7.4 and placed in a graded ethanol series (25%, 50%, 75%, 95%) for 10 min at each step followed by 3 minutes changes in 100% ethanol.

Samples were critical point dried in a Leica Microsystems model EM CPD300 critical point drier (Leica Microsystems, Vienna, Austria) using CO_2 as the transitional fluid. Coverslips were then mounted on aluminum stubs using epoxy glue (System's Three Quick Cure 5, Systems Three Resins, Auburn WA). Samples were coated with osmium at ~10 nm thickness in an NEOC-AT osmium chemical vapor deposition coater (Meiwafosis Co, Osaka, Japan) and examined in a JEOL 7500F (field emission emitter) scanning electron microscope (JEOL, Tokyo, Japan).

$cSiO_2$ phagocytosis assay

To assess phagocytosis of $cSiO_2$ particles, FLAMs, AMs, and BMDMs were seeded at 0.25 cells/cm^2 in 48- or 96-well plates to observe engulfment of surrounding silica particles. The following day, the media was removed, wells were rinsed 1x with sterile PBS, media

replaced with FluoroBrite DMEM (Thermo Fisher) containing 10% FBS and 200 nM SYTOX Green nucleic acid stain (Thermo Fisher). $cSiO_2$ was then added dropwise to a final density of 25–100 μg/cm_2. Cells were imaged over time on an EVOS FL2 fluorescent microscope (Thermo Fisher) with an on-stage, temperature control CO_2 incubator and 2–4 images were acquired per well. SYTOX Green detected on the GFP light cube.

Images were analyzed using analysis pipelines built in the CellProfiler software (33). $cSiO_2$ engulfment was assessed by quantifying the number of $cSiO_2$-filled cells, which have a higher pixel intensity than non-$cSiO_2$-filled cells due to the accumulation of the particles. To avoid counting aggregated $cSiO_2$ particles, a threshold was applied to capture only shapes with high solidity and low compactness. Cell death was quantified by counting SYTOX $Green^+$ cells, respectively.

ELISAs

Cells were treated with $cSiO_2$ for 8 hours or LPS for 24 hours at the indicated concentrations. Cell-free supernatant was collected and the cytokines IL-1α, IL-1β, and IL-10 were analyzed using DuoSet ELISA kits (R&D Systems) per the manufacturer's instructions.

CRISPR Targeted Knockouts

sgRNA cloning sgOpti was a gift from Eric Lander & David Sabatini (Addgene plasmid #85681) (34). Individual sgRNAs were cloned as previously described (35). In short, sgRNA targeting sequences were annealed and phosphorylated then cloned into a dephosphorylated and BsmBI (New England Biolabs) digested SgOpti. sgRNA constructs were then packaged into lentivirus as previously described and used to transduce early passage FLAMs. Two days later, transductants were selected with puromycin. After one week of selection, gDNA was isolated from each targeted FLAM, and PCR was used to amplify edited regions and sanger sequencing was used to quantify indels. Two sgRNAs were targeted per gene and one targeted line was selected for follow up study with editing efficiency >98% for each gene.

Construction of genome-wide loss-of-function library and Siglec-F Screen

The mouse BRIE knockout CRISPR pooled library was a gift of David Root and John Doench (Addgene #73633) (36). Using the BRIE library, 4 sgRNAs targeting every coding gene in mice in addition to 1000 non-targeting controls (78,637 sgRNAs total) were packaged into lentivirus using HEK293T cells and transduced $Cas9^+$ FLAMs at a low multiplicity of infection (MOI <0.3). Two days later these cells were selected with puromycin. We then passaged the transduced library in TGFβ in parallel with non-transduced cells of the same passage without TGFβ. When the non-transduced cells grown in the absence of TGF−β showed reduced Siglec-F expression by flow cytometry we isolated gDNA from the library for sequencing and found high coverage and distribution, with only 1000 sgRNAs not found in the input library. In parallel, the transduced library was fixed, and fluorescence activated cell sorting (FACS) was used to isolate the $SiglecF^{high}$ and $SiglecF^{low}$ bins using a BioRad S3e cell sorter. Genomic DNA was isolated from each sorted population from two biological replicate experiments using a homemade modified salt precipitation method previously described (37). Amplification of sgRNAs by PCR was

performed as previously described using Illumina compatible primers from IDT (36), and amplicons were sequenced on an Illumina NovaSeq 6000 at the RTSF Genomics Core at Michigan State University.

Sequence reads were first trimmed to remove any adapter sequence and to adjust for p5 primer stagger. We used MAGeCK to map reads to the sgRNA library index without allowing for any mismatch. Subsequent sgRNA counts were median normalized to control sgRNAs in MAGeCK to account for variable sequencing depth. To test for sgRNA and gene enrichment, we used the 'test' command in MAGeCK to compare the distribution of sgRNAs in the SiglecF^{high} and SiglecF^{low} bins.

Bioinformatic analysis

Both DAVID analysis and GSEA analysis were used to identify enriched pathways and protein families that were enriched in the data set. Genes were ranked in MAGeCK using RRA and the top enriched positive regulators (4-fold change with at least 2 sgRNAs) were used as a "candidate list" in both DAVID analysis using default settings (38). Functional analysis and functional annotation analysis were completed, and top enriched pathways and protein families were identified. For GSEA analysis, the "GSEA Preranked" function was used to complete functional enrichment using default settings for KEGG, Reactome and GO terms.

Data availability

Raw sequencing data in FASTQ and processed formats will be available for download from NCBI Gene Expression Omnibus (GEO) and available upon request.

Statistical analysis and data visualization

Statistical analysis and data visualization were performed using Prism Version 8 (GraphPad) or R studio as indicated in the figure legends. SYTOX^{+} and $cSiO_2$-filled cells were quantified using CellProfiler. Data are presented, unless otherwise indicated, as the mean ± the standard deviation. For parametric data, one-way ANOVA followed by Tukey's post-hoc test was used to identify significant differences between multiple groups, and Student's t-tests were used to compare two groups. Non-parametric one-way ANOVAs and Mann-Whitney U tests were used to compare multiple groups and two groups, respectively, for non-parametric data.

RESULTS

Fetal liver-derived cells and AMs cultured in GM-CSF alone do not stably express lineage-specific markers over time

The development of a genetically tractable AM *ex vivo* model requires a stable population that maintains AM-like phenotypes and functions long-term. As a first step, we examined the long-term stability of AM-like cells using a previously described method culturing fetal liver derived cells in the cytokine GM-CSF (25). Consistent with previous reports, we found that fetal liver cells grown in GM-CSF phenotypically and morphologically resemble AMs (25, 39, 40). Fetal liver cells grown for 2 weeks *ex vivo* in the presence of GM-CSF adopt a

distinct fried-egg-like morphology akin to AMs (Figure 1A). Scanning electron microscopy revealed that the surfaces of both AM and low passage fetal liver cells (<1 month of culture) have numerous outer membrane ruffles (Figure 1B). However, high passage fetal liver cells (>1 month of culture) underwent a morphological shift from an AM-like, ovoid morphology with numerous outer plasma membrane ruffles, to a smaller, fusiform morphology with loss of membrane ruffles (Figure 1A and 1B). Thus, in our hands, the morphology of fetal liver derived cells grown in recombinant GM-CSF are not stable long-term.

We further examined whether changes in surface markers or gene expression varied as fetal liver cells were cultured over time. Using flow cytometry, we found similarity between AMs and low passage fetal liver cells with high surface expression of Siglec-F and CD11c and low expression of CD14. However, high passage fetal liver cells showed low expression of SiglecF and CD11c, while expressing high levels of CD14 (Figure 1C). Similarly, when we quantified gene expression, we observed that low passage fetal liver cells and AMs express high levels of *Pparg, Car4, Il1a* and *Fabp4* (a transcriptional target of PPARγ) and low levels of CD14, while high passage fetal liver cells expressed very low levels of the AM-associated transcripts but high levels of CD14 (Figure 1D). We observed similar results with AMs isolated from the lungs (Figure S1A and B). To exclude the possibility of contaminating cells outcompeting the alveolar-like cells over long-term culture we used fluorescence activated cell sorting (FACS) to isolate a pure Siglec-F positive population of cells that were then cultured in GM-CSF media. We continued to observe a decline in Siglec-F and CD11c in these cells (Figure S1C). Together these data suggest that prolonged culture of fetal liver-derived cells in GM-CSF media results in a decline in AM-like properties.

Fetal liver-derived cells grown in GM-CSF and TGFβ are phenotypically similar to AMs long-term.

We next pursued strategies to improve the stability of AM-specific phenotypes of fetal liver-derived cells grown *ex vivo*. Based on a prior report that the cytokine TGFβ is critical to AM development and homeostasis (10), we hypothesized that the addition of TGFβ to our culture system would maintain cells in an AM-like state. We first tested whether the addition of TFGβ alters the expression of AM-associated genes. Fetal liver cells in GM-CSF media were treated for 24 hours with 10 ng/mL TGFβ, which we found induced the genes *Pparg, Car4* a transcriptional target of PPAR-γ, and *Itgax* (Figure S2A), all of which are highly expressed by AMs (Figure 1D). We next examined if continued supplementation with TGFβ stabilizes the AM-like phenotypes of fetal liver cells long-term. Fetal liver-derived cells were cultured in GM-CSF media or GM-CSF media containing 20 ng/mL TGFβ. After 15 passages (approximately 2 months of culturing), cells grown in the presence of TGFβ retained a round, AM-like morphology (Figure 2A) and continued expressing AM-identifying genes (Figure 2B). Conversely, fetal liver-derived cells cultured without TGFβ lost the expression of AM-identifying genes *Siglecf, Marco* and *Pparg* and began expressing *Cd14*, which is a common marker for monocyte-derived macrophages recruited to the lung (41) (Figure 2B).

We next determined if fetal liver-derived cells grown in the absence of TGFβ would revert to the AM-like state upon the addition of TGFβ. Fetal liver cells grown in the absence of TGFβ

were cultured with and without TGFβ for 6 days and the expression of Siglec-F and CD14 was quantified by flow cytometry (Figure S2B). In parallel, fetal liver cells maintained in TGFβ were cultured for six days in the presence or absence of TGFβ. We observed that while the removal of TGFβ resulted in a significant decrease in Siglec-F and an increase in CD14, there was no change in expression upon the addition of TGFβ to fetal liver cells that previously lost AM-like marker expression. When we examined the gene expression of *Tgfb1* and the TGFβ receptors, *Tgfbr1* and *Tgfbr2* we observed a significant decrease in expression of the *Tgfb1* (Figure 2B, Figure S2C). These data suggest that the loss of AM-like potential of fetal liver cells grown in the absence of TGFβ is not reversible.

We next quantified changes in the surface expression of Siglec-F and CD14 by flow cytometry in the fetal liver-derived cells grown in the presence and absence of TGFβ. Consistent with our gene expression analysis we observed that fetal liver-derived cells lose the expression of Siglec-F and gain the expression of CD14 over time (Figure 2C and 2D). In contrast, fetal liver-derived cells grown with TGFβ maintained over 80% of cells with high levels of Siglec-F expression and low levels of CD14. Thus, culturing fetal-liver cells in both GM-CSF and TGFβ results in the stable gene expression of self-replicating cells that phenotypically resemble AMs.

Fetal liver-derived cells grown in GM-CSF and TGFβ are functionally similar to AMs in response to $cSiO_2$ relative to phagocytosis, IL-1 cytokine release, and death

To assess the functional similarity of fetal liver-derived cells grown in TGFβ with AMs, we assessed the response of cells to crystalline silica ($cSiO_2$), a respirable particle associated with silicosis and autoimmunity (42, 43). Cells were exposed to various concentrations of $cSiO_2$ for 8 hours. SYTOX Green, a membrane impermeable nucleic acid stain, was included to assess lytic cell death. AMs and low passage fetal liver-derived cells grown with and without TGFβ showed similar rates of $cSiO_2$ engulfment and cell death (Figure 3A). However, late passage fetal liver-derived cells without TGFβ exhibited poor phagocytosis, and as a result, tolerated the presence of $cSiO_2$ without inducing cell death. This unresponsiveness is prevented by TGFβ, as late passage fetal liver-derived cells effectively phagocytosed $cSiO_2$ (Figure 3A and 3B). Rates of phagocytosis by BMDMs were comparable to AMs but were accompanied by a two-fold increase in cell death. Thus, fetal liver-derived cells grown in TGFβ and GM-CSF are functionally stable long-term and recapitulate phagocytosis and cell death kinetics similarly to AMs.

IL-1α is associated with the inflammatory response to particle-induced inflammation. *In vivo* and *ex vivo* studies suggest AMs are the primary source of IL-1α in the lung following inhalation of $cSiO_2$, likely as a result of cell death (44, 45). Initial characterizations of fetal liver-derived cells grown in GM-CSF (30) showed they respond to LPS like AMs by producing high levels of IL-1α and low levels of IL-10 in contrast BMDMs that make little IL-1α. We replicated these experiments and observed similar results with low passage fetal liver-derived cells producing high levels of IL-1α and low levels of IL-10 in response to LPS (Figure S2D). We next tested how the IL-1α response to $cSiO_2$ differed over-time in fetal liver-derived cells grown in the presence and absence of TGFβ. We found that high levels of IL-1α were released both low and high passage fetal liver-derived cells grown in both

GM-CSF and TGFβ following $cSiO_2$ exposure for 8 hours, similar to AMs (Figure 3C). In contrast, we observed that $cSiO_2$ induced IL-1α release from low passage fetal liver-derived cells grown in GM-CSF alone but not late passage cells. Late passage cells grown in GM-CSF alone instead phenocopied BMDMs and released no detectable IL-1α following $cSiO_2$ exposure. Release of IL-1β in these cells may be indicative of inflammasome activation, which is a major mechanism of AM toxicity following exposure to $cSiO_2$. We found $cSiO_2$ exposure to elicit modest IL-1β release from low passage fetal liver-derived cells grown without TGFβ, and from both low and high passage fetal liver-derived cells grown with TGFβ. We further observed a slight, though not significant, increase in IL-1β release in AMs following $cSiO_2$ exposure (Figure 3C). $cSiO_2$-induced IL-1β release was not evident from BMDMs or late MPI cells. Taken together, these experiments show that growth of fetal-liver cells in both GM-CSF and TGFβ recapitulates many aspects of AM physiology and function as stable, long-term, self-propagating cells. We call these cells Fetal Liver-derived Alveolar Macrophages (FLAMs).

CRISPR-Cas9 editing in FLAMs enables disruption of AM-specific responses to cSiO2.

A significant hinderance in the study of AMs is their intractability to standard genetic approaches. This shortcoming has limited the understanding of pathways and regulators that control AM maintenance and function. We hypothesized that FLAMs could be leveraged to dissect AM functional mechanisms. To test this hypothesis we developed CRISPR-Cas9 mediated gene-editing tools by generating FLAMs from Cas9+ mice (46, 47). Using these cells, we targeted *Marco* and *Il1r1*, two genes associated with phagocytosis and inflammatory responses to $cSiO_2$ in AMs (48, 49). Each gene was targeted using two independent sgRNAs per gene by lentiviral transduction. Following selection of successfully transduced cells, we evaluated the editing efficiency of each target genes using Tracking of Indels by DEcomposition (TIDE) analysis. We observed robust editing for both sgRNAs with at least one sgRNA per gene reaching over 95% editing efficiency (see methods). Thus, FLAMs are amenable to genetic targeting by CRISPR-Cas9.

Given the scavenger receptor MARCO has been shown to be involved in $cSiO_2$ uptake and toxicity while IL1R1 is known to amplify inflammatory cues, we hypothesized that cells deficient in MARCO and IL1R1 expression would have a reduced inflammatory response to $cSiO_2$ (48, 50). We therefore tested whether FLAMs targeted for *Marco* or *Il1r1* would differentially respond to $cSiO_2$ exposure compared to wild-type. We exposed control FLAMs and sgMarco or sgIl1r1 FLAMs to two different $cSiO_2$ concentrations and quantified cell death. While we observed no change in cell death in sgIl1r1 FLAMs compared to control FLAMs, a significant reduction in cell death in sgMarco FLAMs was observed following high $cSiO_2$ exposure (Figure 4A). We next examined the production of IL1 following exposure of cells to $cSiO_2$. We found reduced $cSiO_2$-induced IL-1α and IL-1β production by sgMarco and sgIl1r1 FLAMs compared to control FLAMs (Figure 4B,C). Therefore, FLAMs are genetically tractable and can be used to dissect AM-specific functions.

Forward genetic screen in FLAMs identifies regulators of the AM surface marker Siglec-F.

The genetic tractability of FLAMs opens the possibility of performing forward genetic screens in an AM context, which was previously unviable. We recently developed a screening platform in immortalized bone marrow macrophages (iBMDMs) that uses cell sorting of CRISPR-Cas9 targeted cells to enrich for genes that positively or negatively regulate the surface expression of important immune molecules (51). We hypothesized this screening pipeline could be leveraged to dissect pathways responsible for the unique expression profiles seen in AMs and FLAMs. As a first step to test this hypothesis, we dissected the changes in the surface expression of Siglec-F when targeted using CRISPR-Cas9. Among macrophages, Siglec-F is uniquely expressed on the surface of AMs, yet how Siglec-F is regulated remains entirely unknown. Given that Siglec-F expression is lost as cells lose their AM-like phenotypes, globally understanding Siglec-F regulation in FLAMs may inform key gene networks in AMs. To test the dynamic range of Siglec-F expression on FLAMs, we targeted Siglec-F with two independent sgRNAs in both $Cas9^+$ FLAMs and iBMDMs. Again, extensive editing for both sgRNAs was observed with one sgRNA reaching over 99% editing efficiency. As expected, control iBMDMs showed no surface Siglec-F expression and targeting Siglec-F showed no observable change by flow cytometry (Figure 5A). In contrast, we observed robust Siglec-F expression on control FLAMs while sg*SiglecF* FLAMs showed a greater than 100-fold reduction in MFI (Figure 5B). This dynamic range is comparable to other surface markers we previously screened in iBMDMs, suggesting that Siglec-F is an ideal target for a genetic screen in FLAMs (51).

To globally identify genes that contribute to Siglec-F surface expression on FLAMs, we generated a genome-wide knockout library. FLAMs from $Cas9^+$ mice were transduced with sgRNAs from the pooled Brie library (52) which contains 4 independent sgRNAs per mouse coding gene. In parallel to the library, we grew control $Cas9^+$ fetal liver cells with GM-CSF alone to monitor the loss of Siglec-F expression in the absence of TGFβ signaling (Figure 5C and 5D). When control cells lost Siglec-F expression, genomic DNA from the FLAMs knockout library was purified and the sgRNAs were quantified by deep sequencing. The library coverage was confirmed to have minimal skew. We then conducted a forward genetic screen using FACS to isolate the Siglec-F^{high} and Siglec-F^{low} cells from the loss-of-function FLAM library (Figure 5C). Following genomic DNA extraction, sgRNA abundances for each sorted population were determined by deep sequencing. To test for statistical enrichment of sgRNAs and genes, we used the modified robust rank algorithm (α-RRA) employed by Model-based Analysis of Genome-wide CRISPR/Cas9 Knockout (MAGeCK). MAGeCK first ranks sgRNAs by effect and then filters low ranking sgRNAs to improve gene significance testing (53). To identify genes that are required for Siglec-F expression we compared the enrichment of sgRNAs in the Siglec-F^{low} population to the Siglec-F^{high} population. The α-RRA analysis identified over 300 genes with a p-value <0.01 and the second ranked gene in this analysis was the target of the screen Siglec-F (Figure 5E and Table S1). Guide-level analysis showed agreement with all four sgRNAs targeting Siglec-F, with each showing a ten-fold enrichment in the Siglec-F^{low} population (Figure 5F and Table S1). The high ranking of Siglec-F gives high confidence in genome-wide screen results.

Stringent analysis revealed an enrichment of genes with no previously described role in Siglec-F regulation including the TGFβ response regulator USP9x (54) (Figure 6A). To identify pathways that were associated among these genes, we filtered the ranked list to include genes that had a fold change of >4 with at least 2 out of 4 sgRNAs and used DAVID analysis to identify pathways and functions that were enriched in our datasets. The top enriched KEGG pathway was the peroxisome, with all core components of peroxisome biogenesis identified as positive regulators of Siglec-F (Figure 6B). We further examined other peroxisome-associated (PEX) genes and found that 11 out of 15 PEX genes present in our library were altered greater than two-fold (Figure 6C). KEGG pathway analysis identified a significant enrichment in genes associated with lipid metabolism, including glycerophospholipid, inositol phosphate, and ether lipids. KEGG analysis also found an enrichment of the phagosome pathway which identified several surface receptors associated with phagocytosis in this pathway, including the IgG Fc Receptor 4, the mannose-6-phosphate receptor, and the oxidized low-density lipoprotein receptor, suggesting surface proteins associated with phagocytosis directly modulate the stability of Siglec-F (Figure 6D). Examination of enriched UniProt keyword terms using DAVID analysis found a strong enrichment of proteins with oxidoreductase function including several genes associated with cytochromes P450 (CYP), a key regulator of xenobiotic, fatty acid, and hormone metabolism, known to be important in the lung environment (55). Thus, bioinformatic analysis of the top positive regulators of Siglec-F identified pathways that are associated with AM functions.

We next used gene set enrichment analysis (GSEA) to identify functional enrichments from the entire ranked screen dataset. GSEA identified the peroxisome as a top enriched KEGG pathway consistent with the DAVID analysis (Figure 6E). This analysis also identified a strong enrichment for oxidative phosphorylation, which is consistent with the key metabolic changes in AMs compared to BMDMs (56), and a significant enrichment for GPI anchor synthesis as negative regulators of Siglec-F surface expression (Figure 6E). We also noted that mTORC1 signaling was enriched as a negative regulator, in line with previous reports that mTORC1 is required to maintain AMs in the lungs (57). Taken together, our forward genetic screen not only identified Siglec-F,the screen target, but also identified positive and negative regulators of Siglec-F expression that are associated with known AM-functions as well as novel AM regulators. Thus, FLAMs are a tractable genetic platform that enables the detailed interrogation of AM regulatory functions and mechanisms.

DISCUSSION

As long-lived resident macrophages in the lungs, AMs have unique phenotypes and functions shaped by the alveolar environment (58). However, experimental limitations hinder our understanding of AM-specific functional mechanisms. Developing *ex vivo* models that recapitulate AM phenotypes would overcome the challenges associated with isolating and maintaining AMs from the lungs of mice. Since AMs are derived from fetal liver monocytes, previous studies tested the culture of fetal liver cells with GM-CSF (59). These culture conditions result in self-replicating AM-like cells, but in our hands, the AM-like phenotype was not stable long-term. While low passage fetal liver cells grown in GM-CSF are useful for some experimental approaches, the instability of the AM phenotype

precludes functional genetic studies (27, 60). To stabilize the AM-like phenotype of fetal liver-derived cells we supplemented the growth media with TGFβ, a key cytokine for AM maintenance in the lungs, in a model we term FLAMs (10). Here we showed that FLAMs recapitulate many aspects of AM biology, are stable long-term, and are genetically tractable, making them a useful tool to dissect the regulation of AM maintenance and function.

We demonstrated that that even after one month of culture ‘ FLAMs efficiently phagocytose $cSiO_2$ particles, produce inflammatory cytokines like IL-1α, and die similarly to AMs. Our results are consistent with two recent reports that examined how TGFβ modulates macrophages *ex vivo* (10, 27, 60). These reports showed that TGFβ can induce/maintain AM-like phenotypes *ex vivo* using AMs directly from the lungs of mice or purified cells from the bone-marrow. Future studies will be needed to directly compare how distinct sources of AM-like cells grown in GM-CSF and TGFβ are functionally similar or distinct. There are other key differences in these approaches beyond the source of cells, including the use of the PPARγ agonist rosiglitazone. Our data strongly suggest that fetal liver cells do not require rosiglitazone to maintain PPARγ activity. Another advantage of FLAMs is the low cost, low technology threshold and high yield of cells that can be isolated from any genetically modified mouse, including mice with embryonic lethality. Another key advantage of FLAMs is genetic toolbox that we have developed here. Using targeted gene-editing we showed that directed mutations can be easily generated in FLAMs to probe specific AM functions. Furthermore, we generated a genome-wide knockout library in FLAMs and completed the first forward genetic screen in AM-like cells. This proof-of-concept genome-wide screen in FLAMs now enables our innovative tools to be broadly used to understand AM biology in previously impossible detail. Thus, FLAMs recapitulate *ex vivo* AMs even after extended culturing and are suitable for dissecting AM responses and regulation.

How AMs control their functional responses and how this differs from other macrophage populations remains unclear. Here we observed both phenotypic and functional differences among AMs, FLAMs, and BMDMs in line with previous studies (25, 39, 40). While BMDMs express high levels of CD14, AMs and FLAMs express high levels of Siglec-F and MARCO. When cells were exposed to $cSiO_2$, we observed differences in cell death kinetics and IL-1 cytokine responses. Though BMDMs were able to engulf $cSiO_2$ particles at a rate comparable to AMs and FLAMs, they quickly succumbed to cell death, while AMs and FLAMs remained viable many hours following $cSiO_2$ phagocytosis. A delay in cell death may be important for appropriate clearance of particles, potentially allowing the AMs to be transported out of the alveoli before they die (61). AMs and FLAMs cells also released significantly more IL-1α and IL-1β than BMDMs in response to $cSiO_2$. These data are consistent with studies showing high levels of IL-1α produced by AMs compared to other cells in the lung and other macrophage sub-types (25, 39, 44, 45, 59) and the known role of $cSiO_2$ in inducing IL-1β release (49). Our findings indicate that MARCO may be a key player in driving the IL-1 cytokine response in AMs as MARCO-deficient FLAMs showed increased viability and decreased IL-1 production following $cSiO_2$ exposure. These results are in line with previous studies implicating MARCO in the uptake of $cSiO_2$ and other particles in AMs (50, 62). In the future, FLAMs will be used to dissect the underlying mechanisms of MARCO regulation to understand how MARCO drives

distinct inflammatory responses following phagocytosis of $cSiO_2$ and other pathogenic cargo. Knocking out the IL-1 receptor also reduced IL-1 cytokine release, which points to a feed-forward mechanism to amplify this inflammatory response in AMs.

In addition to MARCO, AMs express other markers that are used to define AM populations. However, the regulation of these other AM markers, like Siglec-F, remains entirely unknown. Siglec-F is a surface-expressed immunoglobulin protein that binds sialic acid residues on glycolipids and glycoproteins, but its function in AMs is largely unknown. In addition to AMs, Siglec-F is expressed on eosinophils, where it limits inflammation by modulating cell death pathways (63). The only studies examining Siglec-F in AMs demonstrated that Siglec-F does not regulate phagocytic activity (64). Our forward genetic screen in FLAMs defined regulators of Siglec-F surface expression and uncovered hundreds of candidate genes that may contribute to Siglec-F expression. Our results not only identified Siglec-F as the second ranked candidate, but we identified other genes that likely modulate Siglec-F expression or trafficking. These genes include transcription factors like Fos and NFkB2 and surface receptors like M6PR. Our screen candidates are likely to include both direct regulators of Siglec-F expression and indirect regulators that maintain the AM-like state. In support of this prediction, we identified USP9x, a known regulator of TGFβ signaling as a strong positive regulator of Siglec-F expression (54). In addition, we identified the enrichment of functional pathways previously associated with AM function including the peroxisome, lipid metabolism, oxidative phosphorylation and CYP. Given the previous links among PPAR transcription factors, peroxisome biogenesis, and lipid metabolism, our data strongly suggest FLAMs recapitulate the metabolic makeup of AMs which is central to their gene regulation (12, 56, 65). In further relation to the metabolic state of FLAMs, we identified several CYP family members among our top candidates which regulate vitamin A and all-trans retinoic acid, known modulators of AM function (66, 67). Based on these findings, we posit that PPARγ expression drives lipid metabolism to induce the AM-specific transcriptional profile, resulting in Siglec-F expression. Future studies will be centered on testing this model and deeply validating the genetic screen to uncover novel regulatory mechanisms in FLAMs.

FLAMs are a promising model to study AM biology, yet some limitations remain. While FLAMs maintain many AM-like phenotypes long-term, we observed variable expression of the AM marker CD11c over time. This suggests that there are other signals in addition to GM-CSF and TGFβ that are needed to fully recapitulate AM functionality *ex vivo*. The alveolar space is a highly complex microenvironment, with constant crosstalk between AMs and other cells (58). For example, our data show that FLAMs express TGFβ, yet this is not sufficient to maintain AM-like functions and continued *Tgfbr1* and *Tgfbr2* expression. Given TGFβ is known to amplify *Tgfbr1* and *Tgfbr2* this suggests that the TGFβ produced by FLAMs is not biologically active. *In vivo*, latent TGFβ released by AMs is activated by α-V-β−6 integrins expressed on the type II alveolar epithelial cells (AECII), resulting in increased levels of the active protein which can signal in an autocrine manner to maintain the unique phenotype of AMs (68). This feed-forward loop is absent *ex vivo*, which may explain why addition of exogenous active TGFβ prevents the loss of the AM-like phenotype in FLAMs. Other signals provided by AECII cells and others such as lung-resident basophils likely regulate AM maintenance, but these signals are not modeled in our system (69). In

the future the potential to combine the genetic tractability of FLAMs with *in vivo* transfer models may enable detailed dissection of this cross-regulation systematically. Intranasal transfer of TGFβ-cultured AMs was recently shown to repopulate the alveolar space. It will be important to test if FLAMs could be similarly instilled into lungs lacking endogenous AMs, enabling rapid in vivo studies to better understand AM-maintenance within the lung environment (27).

In summary, we developed FLAMs, a stable *ex vivo* model that can be used to study lung development, immunology, and toxicology. FLAMs are likely to shed new light on processes unique to AMs, like phagocytosis, efferocytosis and the removal of inhaled particles, by employing targeted or genome-wide genetic approaches. Taken together, the optimization and application of FLAMs provides an exciting, innovative model to thoroughly investigate AM biology.

Supplementary Material

Refer to Web version on PubMed Central for supplementary material.

Acknowledgements.

We would like to acknowledge Dr. Jack Harkema, Dr. Melissa Bates, Dr. Mikhail Givralin, Dr. Alexander Misharin, and the members of the Olive and Pestka lab for helpful discussions and input. We thank the MSU flow cytometry core for their help with instrumentation and analysis and Carol Flegler of the MSU Center of Advanced Microscopy for assistance in scanning electron microscopy.

Funding.

This work was supported by startup funding to AJO provided by Michigan State University, the Rackham Endowment Award [AJO], the Dr. Robert and Carol Deibel Family Endowment [JP] as well as grants from the NIH(AI148961 [AJO], F31ES030593 [KW], ES027353 [JP] and T32ES030593 [KW]), DOD (W81XWH2010147 [AJO]) and USDA (NIFA HATCH 1019371 [AJO]).

References

1. Davies LC, Jenkins SJ, Allen JE, and Taylor PR. 2013. Tissue-resident macrophages. Nat Immunol 14: 986–995. [PubMed: 24048120]
2. Mass E, Ballesteros I, Farlik M, Halbritter F, Gunther P, Crozet L, Jacome-Galarza CE, Handler K, Klughammer J, Kobayashi Y, Gomez-Perdiguero E, Schultze JL, Beyer M, Bock C, and Geissmann F. 2016. Specification of tissue-resident macrophages during organogenesis. Science 353.
3. Lavin Y, Winter D, Blecher-Gonen R, David E, Keren-Shaul H, Merad M, Jung S, and Amit I. 2014. Tissue-resident macrophage enhancer landscapes are shaped by the local microenvironment. Cell 159: 1312–1326. [PubMed: 25480296]
4. Hetzel M, Ackermann M, and Lachmann N. 2021. Beyond “Big Eaters”: The versatile role of alveolar macrophages in health and disease. Int J Mol Sci 22. [PubMed: 35008458]
5. Reddy RC, Keshamouni VG, Jaigirdar SH, Zeng X, Leff T, Thannickal VJ, and Standiford TJ. 2004. Deactivation of murine alveolar macrophages by peroxisome proliferator-activated receptor-gamma ligands. American journal of physiology. Lung cellular and molecular physiology 286.
6. Misharin A. v, Morales-Nebreda L, Mutlu GM, Budinger GR, and Perlman H. 2013. Flow cytometric analysis of macrophages and dendritic cell subsets in the mouse lung. Am J Respir Cell Mol Biol 49: 503–510. [PubMed: 23672262]
7. Guilliams M, de Kleer I, Henri S, Post S, Vanhoutte L, de Prijck S, Deswarte K, Malissen B, Hammad H, and Lambrecht BN. 2013. Alveolar macrophages develop from fetal monocytes that

differentiate into long-lived cells in the first week of life via GM-CSF. J Exp Med 210: 1977–1992. [PubMed: 24043763]

8. Kopf M, Schneider C, and Nobs SP. 2015. The development and function of lung-resident macrophages and dendritic cells. Nat Immunol 16: 36–44. [PubMed: 25521683]
9. Ginhoux F, and Guilliams M. 2016. Tissue-resident macrophage ontogeny and homeostasis. Immunity 44: 439–449. [PubMed: 26982352]
10. Yu X, Buttgereit A, Lelios I, Utz SG, Cansever D, Becher B, and Greter M. 2017. The Cytokine TGF-beta Promotes the Development and Homeostasis of Alveolar Macrophages. Immunity 47: 903–912 e4. [PubMed: 29126797]
11. Schneider C, Nobs SP, Kurrer M, Rehrauer H, Thiele C, and Kopf M. 2014. Induction of the nuclear receptor PPAR-gamma by the cytokine GM-CSF is critical for the differentiation of fetal monocytes into alveolar macrophages. Nat Immunol 15: 1026–1037. [PubMed: 25263125]
12. Reddy RC 2008. Immunomodulatory role of PPAR-gamma in alveolar macrophages. J Investig Med 56: 522–527.
13. Bonfield TL, Farver CF, Barna BP, Malur A, Abraham S, Raychaudhuri B, Kavuru MS, and Thomassen MJ. 2003. Peroxisome proliferator-activated receptor-gamma is deficient in alveolar macrophages from patients with alveolar proteinosis. Am J Respir Cell Mol Biol 29: 677–682. [PubMed: 12805087]
14. Trapnell BC, Nakata K, Bonella F, Campo I, Griese M, Hamilton J, Wang T, Morgan C, Cottin V, and McCarthy C. 2019. Pulmonary alveolar proteinosis. Nature Reviews Disease Primers 2019 5:1 5: 1–17.
15. Berenson C, Kruzel R, Eberhardt E, and Sethi S. 2013. Phagocytic dysfunction of human alveolar macrophages and severity of chronic obstructive pulmonary disease. The Journal of infectious diseases 208: 2036–2045. [PubMed: 23908477]
16. Berenson CS, Kruzel RL, Eberhardt E, Dolnick R, Minderman H, Wallace PK, and Sethi S. 2014. Impaired innate immune alveolar macrophage response and the predilection for COPD exacerbations. Thorax.
17. Liang Z, Zhang Q, Thomas CM, Chana KK, Gibeon D, Barnes PJ, Chung KF, Bhavsar PK, and Donnelly LE. 2014. Impaired macrophage phagocytosis of bacteria in severe asthma. Respiratory Research 2014 15:1 15: 1–11.
18. Lévêque M, le Trionnaire S, del Porto P, and Martin-Chouly C. 2017. The impact of impaired macrophage functions in cystic fibrosis disease progression. Journal of Cystic Fibrosis 16: 443–453. [PubMed: 27856165]
19. McCubbrey A, and Curtis J. 2013. Efferocytosis and lung disease. Chest 143: 1750–1757. [PubMed: 23732585]
20. Busch CJ, Favret J, Geirsdottir L, Molawi K, and Sieweke MH. 2019. Isolation and long-term cultivation of mouse alveolar macrophages. Bio Protoc 9.
21. Chen YW, Huang MZ, Chen CL, Kuo CY, Yang CY, Chiang-Ni C, Chen YM, Hsieh CM, Wu HY, Kuo ML, Chiu CH, and Lai CH. 2020. PM2.5 impairs macrophage functions to exacerbate pneumococcus-induced pulmonary pathogenesis. Part Fibre Toxicol 17: 37. [PubMed: 32753046]
22. Dostert C, Petrilli V, van Bruggen R, Steele C, Mossman BT, and Tschopp J. 2008. Innate immune activation through Nalp3 inflammasome sensing of asbestos and silica. Science 320: 674–677. [PubMed: 18403674]
23. Hornung V, Bauernfeind F, Halle A, Samstad EO, Kono H, Rock KL, Fitzgerald KA, and Latz E. 2008. Silica crystals and aluminum salts activate the NALP3 inflammasome through phagosomal destabilization. Nature Immunology 9: 847–856. [PubMed: 18604214]
24. Brenner TA, Rice TA, Anderson ED, Percopo CM, and Rosenberg HF. 2016. Immortalized MH-S cells lack defining features of primary alveolar macrophages and do not support mouse pneumovirus replication. Immunol Lett 172: 106–112. [PubMed: 26916143]
25. Fejer G, Wegner MD, Gyory I, Cohen I, Engelhard P, Voronov E, Manke T, Ruzsics Z, Dolken L, Prazeres da Costa O, Branzk N, Huber M, Prasse A, Schneider R, Apte RN, Galanos C, and Freudenberg MA. 2013. Nontransformed, GM-CSF-dependent macrophage lines are a unique model to study tissue macrophage functions. Proc Natl Acad Sci U S A 110: E2191–8. [PubMed: 23708119]

26. Wierenga KA, Wee J, Gilley KN, Rajasinghe LD, Bates MA, Gavrilin MA, Holian A, and Pestka JJ. 2019. Docosahexaenoic acid suppresses silica-induced inflammasome activation and IL-1 cytokine release by interfering with priming signal. Frontiers in Immunology 10.
27. Gorki A, Symmank D, Zahalka S, Lakovits K, Hladik A, Langer B, Maurer B, Sexl V, Kain R, and Knapp S. 2021. Murine ex vivo Cultured Alveolar Macrophages Provide a Novel Tool to Study Tissue-Resident Macrophage Behavior and Function. American Journal of Respiratory Cell and Molecular Biology.
28. Bates MA, Brandenberger C, Langohr I, Kumagai K, Harkema JR, Holian A, and Pestka JJ. 2015. Silica triggers inflammation and ectopic lymphoid neogenesis in the lungs in parallel with accelerated onset of systemic autoimmunity and glomerulonephritis in the lupus-prone NZBWF1 mouse. PLoS ONE 10.
29. Bates MA, Akbari P, Gilley KN, Wagner JG, Li N, Kopec AK, Wierenga KA, Jackson-Humbles D, Brandenberger C, Holian A, Benninghoff AD, Harkema JR, and Pestka JJ. 2018. Dietary docosahexaenoic acid prevents silica-induced development of pulmonary ectopic germinal centers and glomerulonephritis in the lupus-prone NZBWF1 mouse. Front Immunol 9: 2002. [PubMed: 30258439]
30. Fejer G, Wegner MD, Gyory I, Cohen I, Engelhard P, Voronov E, Manke T, Ruzsics Z, Dolken L, Prazeres da Costa O, Branzk N, Huber M, Prasse A, Schneider R, Apte RN, Galanos C, and Freudenberg MA. 2013. Nontransformed, GM-CSF-dependent macrophage lines are a unique model to study tissue macrophage functions. Proc Natl Acad Sci U S A 110: E2191–8. [PubMed: 23708119]
31. Weischenfeldt J, and Porse B. 2008. Bone marrow-derived macrophages (BMM): Isolation and applications. Cold Spring Harbor Protocols 3.
32. Fahy RJ, Exline MC, Gavrilin MA, Bhatt NY, Besecker BY, Sarkar A, Hollyfield JL, Duncan MD, Nagaraja HN, Knatz NL, Hall M, and Wewers MD. 2008. Inflammasome mRNA expression in human monocytes during early septic shock. Am J Respir Crit Care Med 177: 983–988. [PubMed: 18263805]
33. Carpenter AE, Jones TR, Lamprecht MR, Clarke C, Kang IH, Friman O, Guertin DA, Chang JH, Lindquist RA, Moffat J, Golland P, and Sabatini DM. 2006. CellProfiler: image analysis software for identifying and quantifying cell phenotypes. Genome Biol 7: R100. [PubMed: 17076895]
34. Fulco CP, Munschauer M, Anyoha R, Munson G, Grossman SR, Perez EM, Kane M, Cleary B, Lander ES, and Engreitz JM. 2016. Systematic mapping of functional enhancer-promoter connections with CRISPR interference. Science 354: 769–773. [PubMed: 27708057]
35. Shalem O, Sanjana NE, Hartenian E, Shi X, Scott DA, Mikkelsen TS, Heckl D, Ebert BL, Root DE, Doench JG, and Zhang F. 2014. Genome-scale CRISPR-Cas9 knockout screening in human cells. Science (New York, N.Y.) 343: 84–87. [PubMed: 24336571]
36. Doench JG, Fusi N, Sullender M, Hegde M, Vaimberg EW, Donovan KF, Smith I, Tothova Z, Wilen C, Orchard R, Virgin HW, Listgarten J, and Root DE. 2016. Optimized sgRNA design to maximize activity and minimize off-target effects of CRISPR-Cas9. Nat Biotechnol 34: 184–191. [PubMed: 26780180]
37. Chen S, Sanjana NE, Zheng K, Shalem O, Lee K, Shi X, Scott DA, Song J, Pan JQ, Weissleder R, Lee H, Zhang F, and Sharp PA. 2015. Genome-wide CRISPR screen in a mouse model of tumor growth and metastasis. Cell 160: 1246. [PubMed: 25748654]
38. Huang DW, Sherman BT, and Lempicki RA. 2009. Systematic and integrative analysis of large gene lists using DAVID bioinformatics resources. Nature protocols 4: 44–57. [PubMed: 19131956]
39. Maler MD, Nielsen PJ, Stichling N, Cohen I, Ruzsics Z, Wood C, Engelhard P, Suomalainen M, Gyory I, Huber M, Muller-Quernheim J, Schamel WWA, Gordon S, Jakob T, Martin SF, Jahnen-Dechent W, Greber UF, Freudenberg MA, and Fejer G. 2017. Key role of the scavenger receptor MARCO in mediating adenovirus infection and subsequent innate responses of macrophages. mBio 8.
40. Woo M, Wood C, Kwon D, Park KP, Fejer G, and Delorme V. 2018. Mycobacterium tuberculosis infection and innate responses in a new model of lung alveolar macrophages. Front Immunol 9: 438. [PubMed: 29593716]
41. Mould KJ, Jackson ND, Henson PM, Seibold M, and Janssen WJ. 2019. Single cell RNA sequencing identifies unique inflammatory airspace macrophage subsets. JCI Insight 4.

42. Pollard KM 2016. Silica, silicosis, and autoimmunity. Frontiers in Immunology 7. [PubMed: 26834748]
43. Parks CG, Miller FW, Pollard KM, Selmi C, Germolec D, Joyce K, Rose NR, and Humble MC. 2014. Expert panel workshop consensus statement on the role of the environment in the development of autoimmune disease. Int J Mol Sci 15: 14269–14297. [PubMed: 25196523]
44. Kuroda E, Ozasa K, Temizoz B, Ohata K, Koo CX, Kanuma T, Kusakabe T, Kobari S, Horie M, Morimoto Y, Nakajima S, Kabashima K, Ziegler SF, Iwakura Y, Ise W, Kurosaki T, Nagatake T, Kunisawa J, Takemura N, Uematsu S, Hayashi M, Aoshi T, Kobiyama K, Coban C, and Ishii KJ. 2016. Inhaled fine particles induce alveolar macrophage death and interleukin-1alpha release to promote inducible bronchus-associated lymphoid tissue formation. Immunity 45: 1299–1310. [PubMed: 28002730]
45. Rabolli V, Badissi AA, Devosse R, Uwambayinema F, Yakoub Y, Palmai-Pallag M, Lebrun A, de Gussem V, Couillin I, Ryffel B, Marbaix E, Lison D, and Huaux F. 2014. The alarmin IL-1alpha is a master cytokine in acute lung inflammation induced by silica micro- and nanoparticles. Part Fibre Toxicol 11: 69. [PubMed: 25497724]
46. Platt RJ, Chen S, Zhou Y, Yim MJ, Swiech L, Kempton HR, Dahlman JE, Parnas O, Eisenhaure TM, Jovanovic M, Graham DB, Jhunjhunwala S, Heidenreich M, Xavier RJ, Langer R, Anderson DG, Hacohen N, Regev A, Feng G, Sharp PA, and Zhang F. 2014. CRISPR-Cas9 knockin mice for genome editing and cancer modeling. Cell 159: 440–455. [PubMed: 25263330]
47. Cortez JT, Montauti E, Shifrut E, Gatchalian J, Zhang Y, Shaked O, Xu Y, Roth TL, Simeonov DR, Zhang Y, Chen S, Li Z, Woo JM, Ho J, Vogel IA, Prator GY, Zhang B, Lee Y, Sun Z, Ifergan I, van Gool F, Hargreaves DC, Bluestone JA, Marson A, and Fang D. 2020. CRISPR screen in regulatory T cells reveals modulators of Foxp3. Nature 582: 416–420. [PubMed: 32499641]
48. Thakur SA, Beamer CA, Migliaccio CT, and Holian A. 2009. Critical role of MARCO in crystalline silica-induced pulmonary inflammation. Toxicol Sci 108: 462–471. [PubMed: 19151164]
49. Hornung V, Bauernfeind F, Halle A, Samstad EO, Kono H, Rock KL, Fitzgerald KA, and Latz E. 2008. Silica crystals and aluminum salts activate the NALP3 inflammasome through phagosomal destabilization. Nat Immunol 9: 847–856. [PubMed: 18604214]
50. Hamilton RF Jr., Thakur SA, Mayfair JK, and Holian A. 2006. MARCO mediates silica uptake and toxicity in alveolar macrophages from C57BL/6 mice. J Biol Chem 281: 34218–34226. [PubMed: 16984918]
51. Kiritsy MC, Ankley LM, Trombley J, Huizinga GP, Lord AE, Orning P, Elling R, Fitzgerald KA, and Olive AJ. 2021. A genetic screen in macrophages identifies new regulators of IFNγ-inducible MHCII that contribute to T cell activation. eLife 10.
52. Sanson KR, Hanna RE, Hegde M, Donovan KF, Strand C, Sullender ME, Vaimberg EW, Goodale A, Root DE, Piccioni F, and Doench JG. 2018. Optimized libraries for CRISPR-Cas9 genetic screens with multiple modalities. Nature Communications 2018 9:1 9: 1–15.
53. Li W, Xu H, Xiao T, Cong L, Love MI, Zhang F, Irizarry RA, Liu JS, Brown M, and Liu XS. 2014. MAGeCK enables robust identification of essential genes from genome-scale CRISPR/Cas9 knockout screens. Genome biology 15: 554. [PubMed: 25476604]
54. Dupont S, Mamidi A, Cordenonsi M, Montagner M, Zacchigna L, Adorno M, Martello G, Stinchfield MJ, Soligo S, Morsut L, Inui M, Moro S, Modena N, Argenton F, Newfeld SJ, and Piccolo S. 2009. FAM/USP9x, a deubiquitinating enzyme essential for TGFbeta signaling, controls Smad4 monoubiquitination. Cell 136: 123–135. [PubMed: 19135894]
55. Esteves F, Rueff J, and Kranendonk M. 2021. The Central Role of Cytochrome P450 in Xenobiotic Metabolism-A Brief Review on a Fascinating Enzyme Family. Journal of xenobiotics 11: 94–114. [PubMed: 34206277]
56. Woods PS, Kimmig LM, Meliton AY, Sun KA, Tian Y, O'Leary EM, Gökalp GA, Hamanaka RB, and Mutlu GM. 2020. Tissue-resident alveolar macrophages do not rely on glycolysis for LPS-induced inflammation. American Journal of Respiratory Cell and Molecular Biology 62: 243–255. [PubMed: 31469581]
57. Sinclair C, Bommakanti G, Gardinassi L, Loebbermann J, Johnson MJ, Hakimpour P, Hagan T, Benitez L, Todor A, Machiah D, Oriss T, Ray A, Bosinger S, Ravindran R, Li S, and Pulendran

B. 2017. mTOR regulates metabolic adaptation of APCs in the lung and controls the outcome of allergic inflammation. Science (New York, N.Y.) 357: 1014–1021. [PubMed: 28798047]

58. Bissonnette EY, Lauzon-Joset JF, Debley JS, and Ziegler SF. 2020. Cross-Talk Between Alveolar Macrophages and Lung Epithelial Cells is Essential to Maintain Lung Homeostasis. Front Immunol 11: 583042. [PubMed: 33178214]
59. Fejer G, Sharma S, and Gyory I. 2015. Self-renewing macrophages--a new line of enquiries in mononuclear phagocytes. Immunobiology 220: 169–174. [PubMed: 25468723]
60. Luo M, Lai W, He Z, and Wu L. 2021. Development of an Optimized Culture System for Generating Mouse Alveolar Macrophage–like Cells. The Journal of Immunology 207: 1683–1693. [PubMed: 34400525]
61. Kawasaki H 2015. A mechanistic review of silica-induced inhalation toxicity. Inhalation Toxicology 27: 363–377. [PubMed: 26194035]
62. Arredouani MS, Palecanda A, Koziel H, Huang YC, Imrich A, Sulahian TH, Ning YY, Yang Z, Pikkarainen T, Sankala M, Vargas SO, Takeya M, Tryggvason K, and Kobzik L. 2005. MARCO is the major binding receptor for unopsonized particles and bacteria on human alveolar macrophages. J Immunol 175: 6058–6064. [PubMed: 16237101]
63. Mao H, Kano G, Hudson SA, Brummet M, Zimmermann N, Zhu Z, and Bochner BS. 2013. Mechanisms of Siglec-F-Induced Eosinophil Apoptosis: A Role for Caspases but Not for SHP-1, Src Kinases, NADPH Oxidase or Reactive Oxygen. PLOS ONE 8: e68143. [PubMed: 23840825]
64. Feng YH, and Mao H. 2012. Expression and preliminary functional analysis of Siglec-F on mouse macrophages. Journal of Zhejiang University. Science. B 13: 386. [PubMed: 22556177]
65. Ginhoux F 2014. Fate PPAR-titioning: PPAR-gamma “instructs” alveolar macrophage development. Nat Immunol 15: 1005–1007. [PubMed: 25329182]
66. Coleman MM, Ruane D, Moran B, Dunne PJ, Keane J, and Mills KHG. 2013. Alveolar macrophages contribute to respiratory tolerance by inducing FoxP3 expression in naive T cells. American Journal of Respiratory Cell and Molecular Biology 48: 773–780. [PubMed: 23492186]
67. Li S, Lei Y, Lei J, and Li H. 2021. All-trans retinoic acid promotes macrophage phagocytosis and decreases inflammation via inhibiting CD14/TLR4 in acute lung injury. Molecular medicine reports 24.
68. Munger JS, Huang X, Kawakatsu H, Griffiths MJD, Dalton SL, Wu J, Pittet JF, Kaminski N, Garat C, Matthay MA, Rifkin DB, and Sheppard D. 1999. A Mechanism for Regulating Pulmonary Inflammation and Fibrosis: The Integrin αvβ6 Binds and Activates Latent TGF β1. Cell 96: 319–328. [PubMed: 10025398]
69. Kannan S, Huang H, Seeger D, Audet A, Chen Y, Huang C, Gao H, Li S, and Wu M. 2009. Alveolar epithelial type II cells activate alveolar macrophages and mitigate P. Aeruginosa infection. PloS one 4.

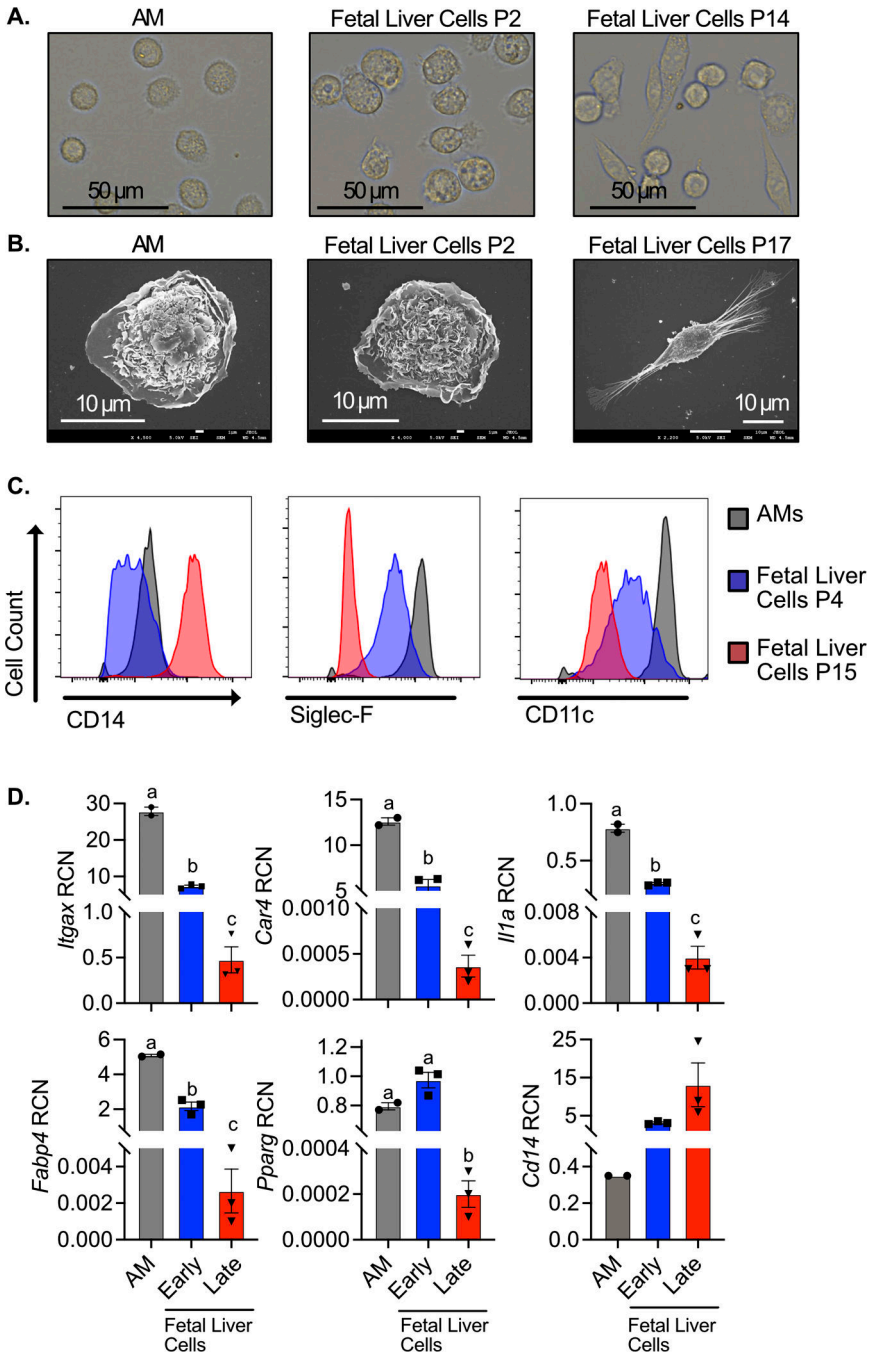

Figure 1. Fetal liver macrophages cultured with GM-CSF lose their AM-like phenotype over time.

Fetal liver cells were cultured with GM-CSF and analyzed at indicated passage. AMs were isolated and analyzed immediately. **A)** AMs, P2 fetal liver cells, and P37 fetal liver cells were lifted from culture and imaged on a EVOS FL Auto 2 fluorescent microscope at 60x magnification. **B)** AMs, P3 fetal liver cells, and P15 fetal liver cells were fixed and imaged by scanning electron microscopy at 4500x, 4000x, and 2200x, respectively. **C)** Alveolar macrophages (Gray), P4 fetal liver macrophages (Blue), and P15 fetal liver

macrophages (Red) were assessed for surface expression of the markers CD14, Siglec-F, and CD11c by flow cytometry. **D)** Gene expression of indicated genes in AMs, early fetal liver macrophages (P1), and late fetal liver macrophages (P18) was quantified by qPCR. Data was compared using one-way ANOVA followed by Tukey's multiple comparisons test. Bars labeled with unique letters are significantly different *($p<0.05$).* Results are representative of 2 or 3 independent experiments.

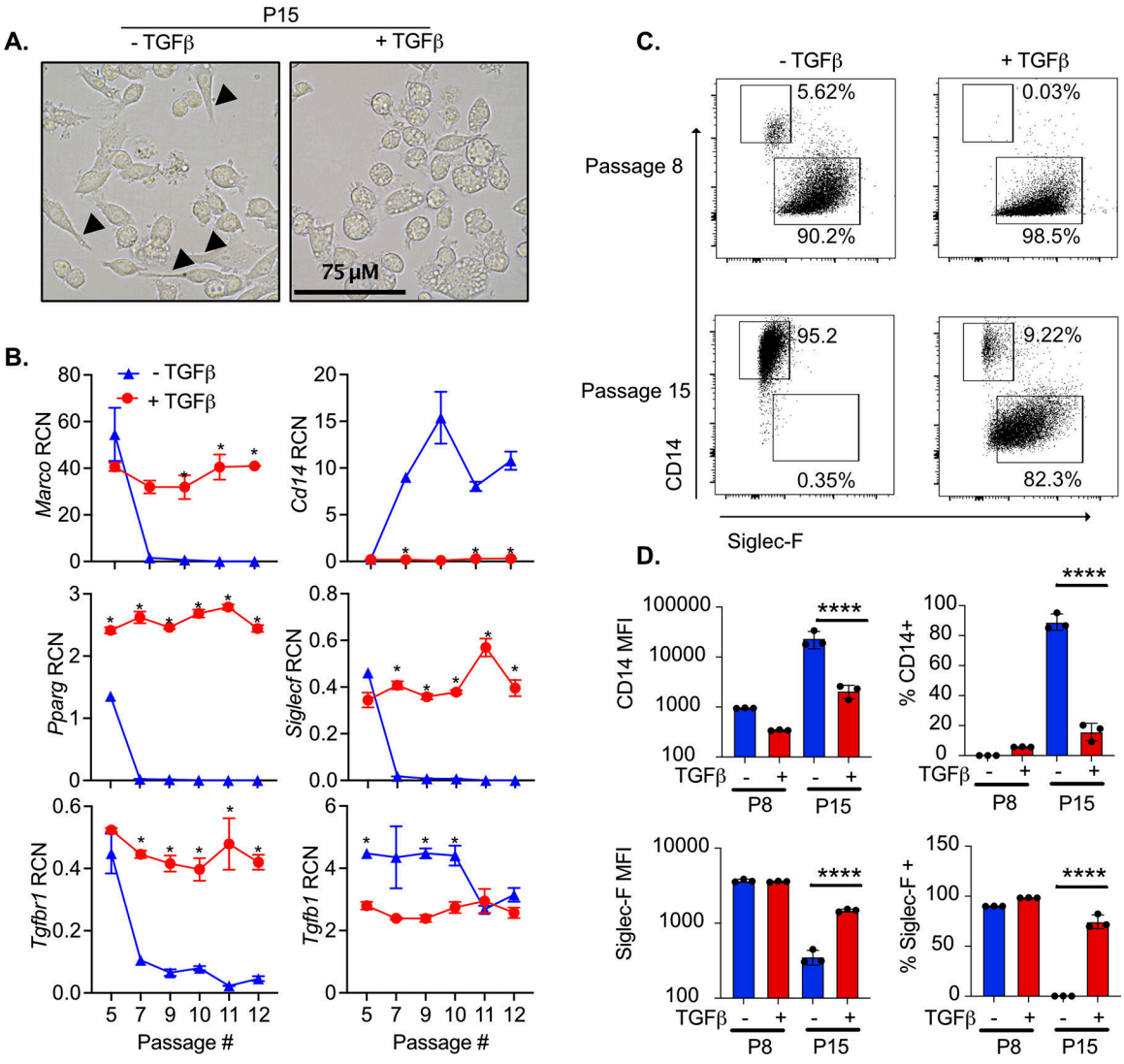

Figure 2. Culturing fetal liver cells with TGFβ and GM-CSF maintains AM-like phenotypes long-term.

Fetal liver cells were cultured with or without TGFβ for the indicated passages. **A)** P15 cells cultured with and without TGFβ were imaged on a EVOS FL Auto 2 fluorescent microscope at 60x magnification. Cells with a clearly visible spindleoid morphology are marked with arrows. **B)** At the indicated passage, RNA was extracted from a subset of cells for gene expression analysis. Expression of the indicated genes are quantified as relative copy number (RCN) compared to *Gapdh*. Asterisks indicate significant (p<0.05) differences in gene expression of cells cultured with and without TGF-β cells at the same passage number, as determined by Student's t-test. **C)** At the indicated passage, cells were analyzed by flow cytometry for the surface expression of CD14 and Siglec-F. Representative biaxial plots from triplicate samples is shown. **D)** Quantification of the mean fluorescence intensity (MFI) and percent of cells positive of CD14 and Siglec-F surface expression from cells in (C) expressed as MFI (left) and percent positive (right). Results are representative of at least two independent experiments. ****p<.0001 by one-way ANOVA with a Tukey correction for multiple comparisons.

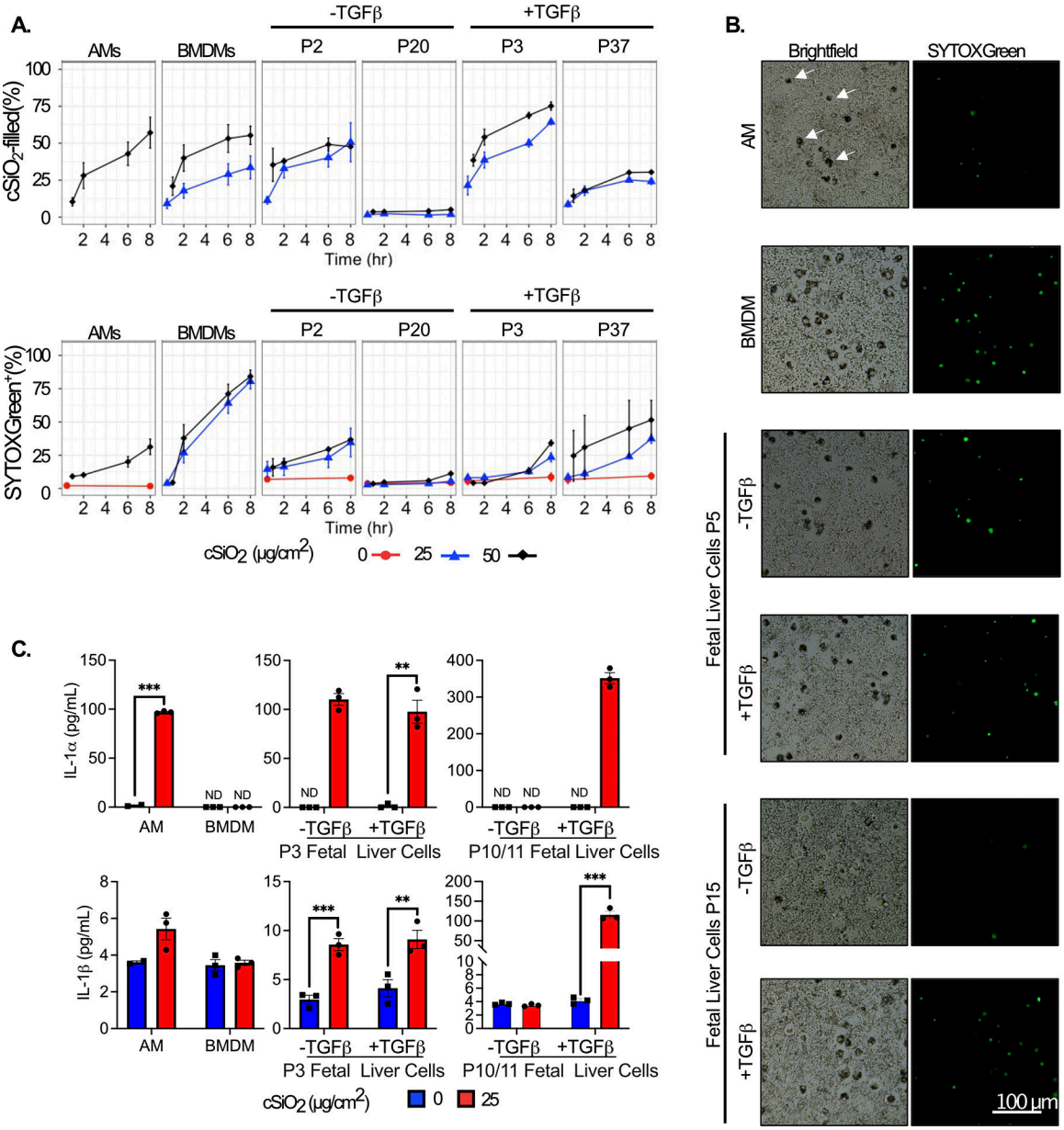

Figure 3. The kinetics of $cSiO_2$ uptake and $cSiO_2$-induced cell death and IL-1 release are similar among AMs and FLAMs.

AMs, bone marrow-derived macrophages (BMDMs), and fetal liver cells were seeded in 96-well plates. After 24 hours, media was replaced with FluoroBrite DMEM containing 200 nM SYTOX green and 10% FBS. $cSiO_2$ at the indicated densities was added dropwise to cells and images were taken at 0, 2, 6, and 8 hours using an EVOS FL2 fluorescent microscope. **A)** The percent of $cSiO_2$-filled and $SYTOX^+$ cells were quantified using the CellProfiler software. **B)** Representative images of $SYTOX^+$ and $cSiO_2$-filled cells (white arrows in AM panel, top right) treated with 50 μg/cm^2 silica for 8 hours, 20x magnification. **C)** In a separate experiment, the supernatant was collected after 8 hr treatment with 25 μg/cm^2 to assess release of the cytokines IL-1α **(Top)** and IL-1β **(Bottom)** by ELISA. Asterisks indicative of significant differences between groups (**p<0.01, ***p<0.001), as assessed by

Student’s t-tests between relevant groups. ND = not detected. Results are representative of at least two independent experiments.

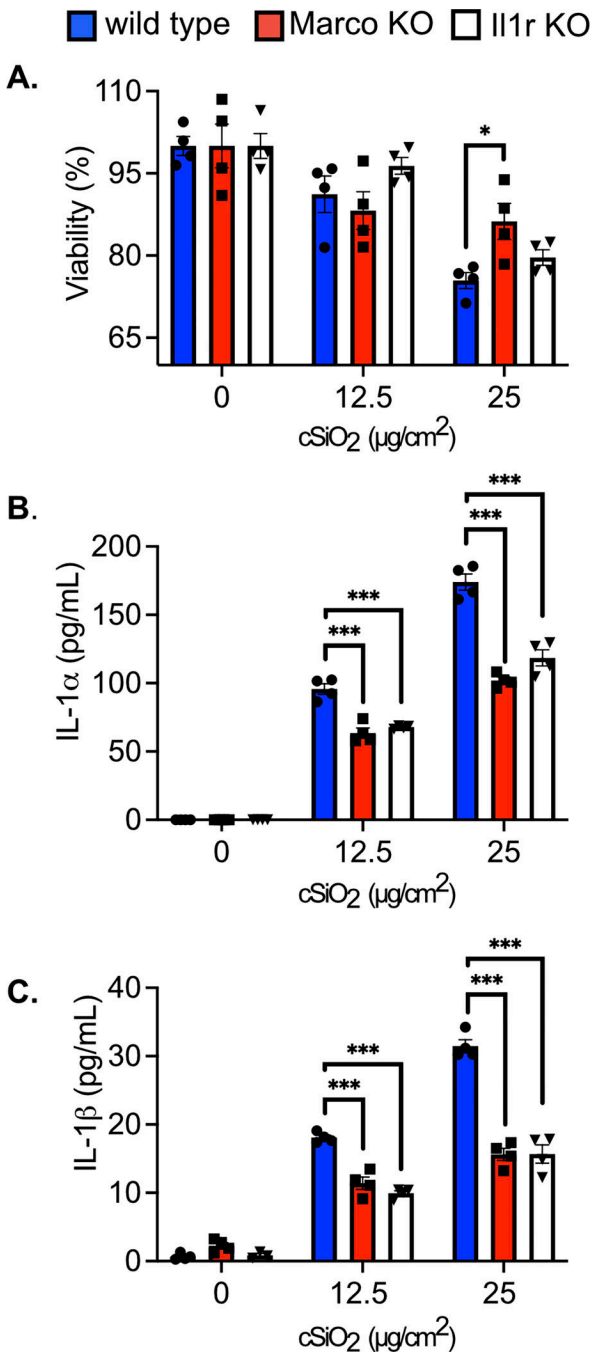

Figure 4. The loss of *Marco* and *Il1r* modulate the response of FLAMs to $cSiO_2$ treatment.
Wild type, *Marco* KO, and *Il1r1* KO FLAMs were treated with $cSiO_2$ at the indicated concentrations for 8 hours. A) Cell viability was determined using the MTS assay, with 100% viability determined as the mean absorbance of the formazan dye product in the untreated WT cells. Supernatant was collected to measure release of B) IL-1α and C) IL-1β. Asterisks indicate significant differences (*p<0.05, ***p<0.001) between cell types within treatment groups, as determined by one-way ANOVA. Results are representative of at least two independent experiments with biological triplicates.

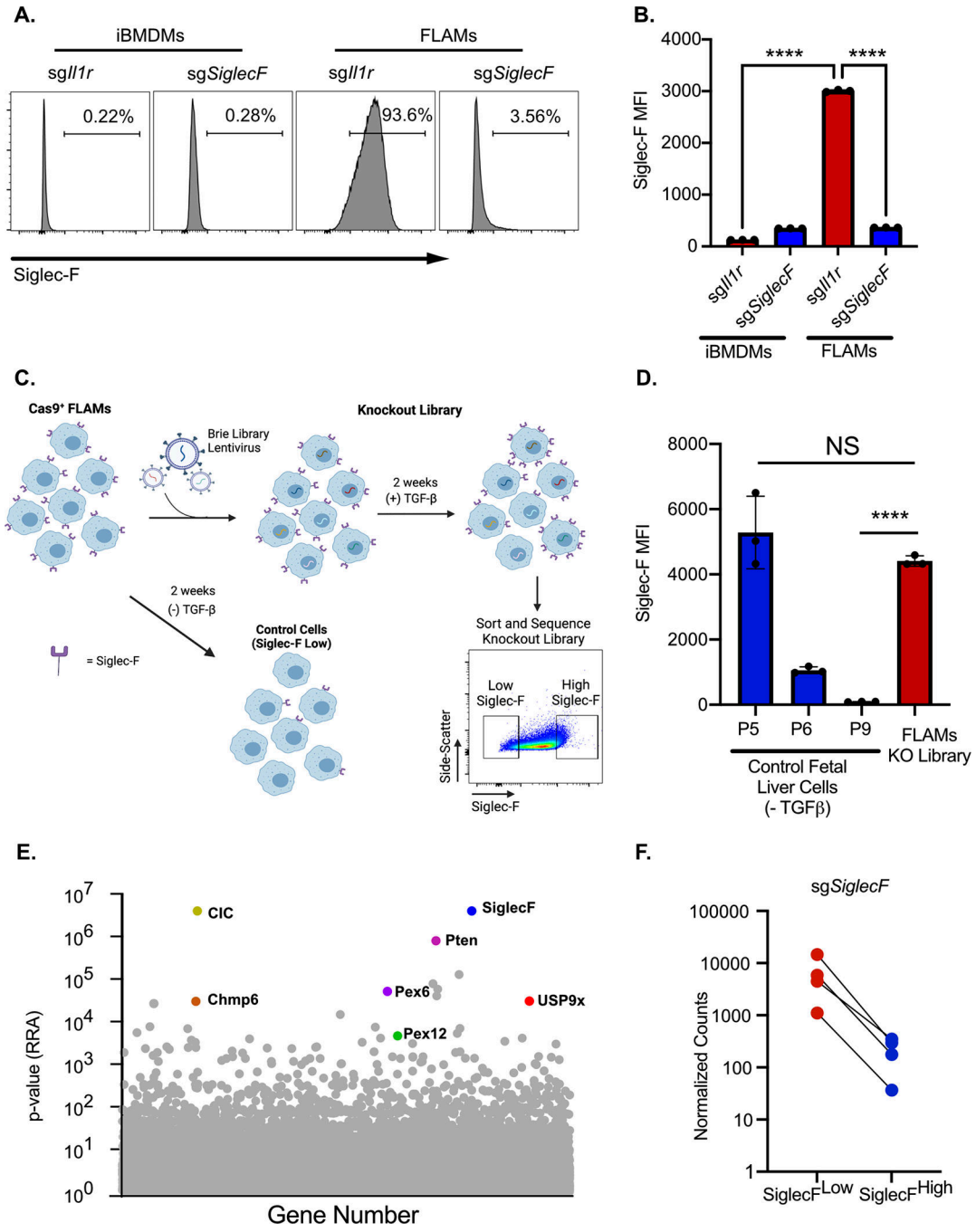

Figure 5. A loss-of-function forward genetic screen identifies regulators of Siglec-F surface expression on FLAMs.

iBMDMs or FLAMs targeted for *Il1r1* or *SiglecF* were analyzed by flow cytometry for Siglec-F surface expression. A) Shown are representative histograms of surface expression. **B)** The MFI of Siglec-F surface expression was quantified on cells of the indicated genotypes. ****$p<0.0001$ between samples by one-way ANOVA with a Tukey correction. These data are representative of two independent experiments **C)** Shown is a schematic of the generation of the FLAM knockout library and screen to identify Siglec-F regulators.

The transduction of Cas9+ FLAMs with genome-wide library of sgRNAs results in variable Siglec-F surface expression. When parallel control FLAMs grown in the absence of TGFβ lost Siglec-F expression the top and bottom 5% of Siglec-F expression cells were isolated from the knockout FLAM library by FACS. Sorted cells were then used for downstream sequencing and analysis. **D)** Siglec-F surface expression of library control cells grown in the absence of TGFβ was monitored over time and compared to the transduced FLAM library prior to sorting. Shown is the MFI for Siglec-F expression of the indicated cells and passage numbers **E)** Shown is the α-RRA score of each gene in CRISPR library that passed filtering metrics in MAGeCK. Genes of interest are noted. **F)** Normalized sg*SiglecF* counts for each sgRNA found in both the SiglecF^{low} and SiglecF^{high} sorted populations is shown.

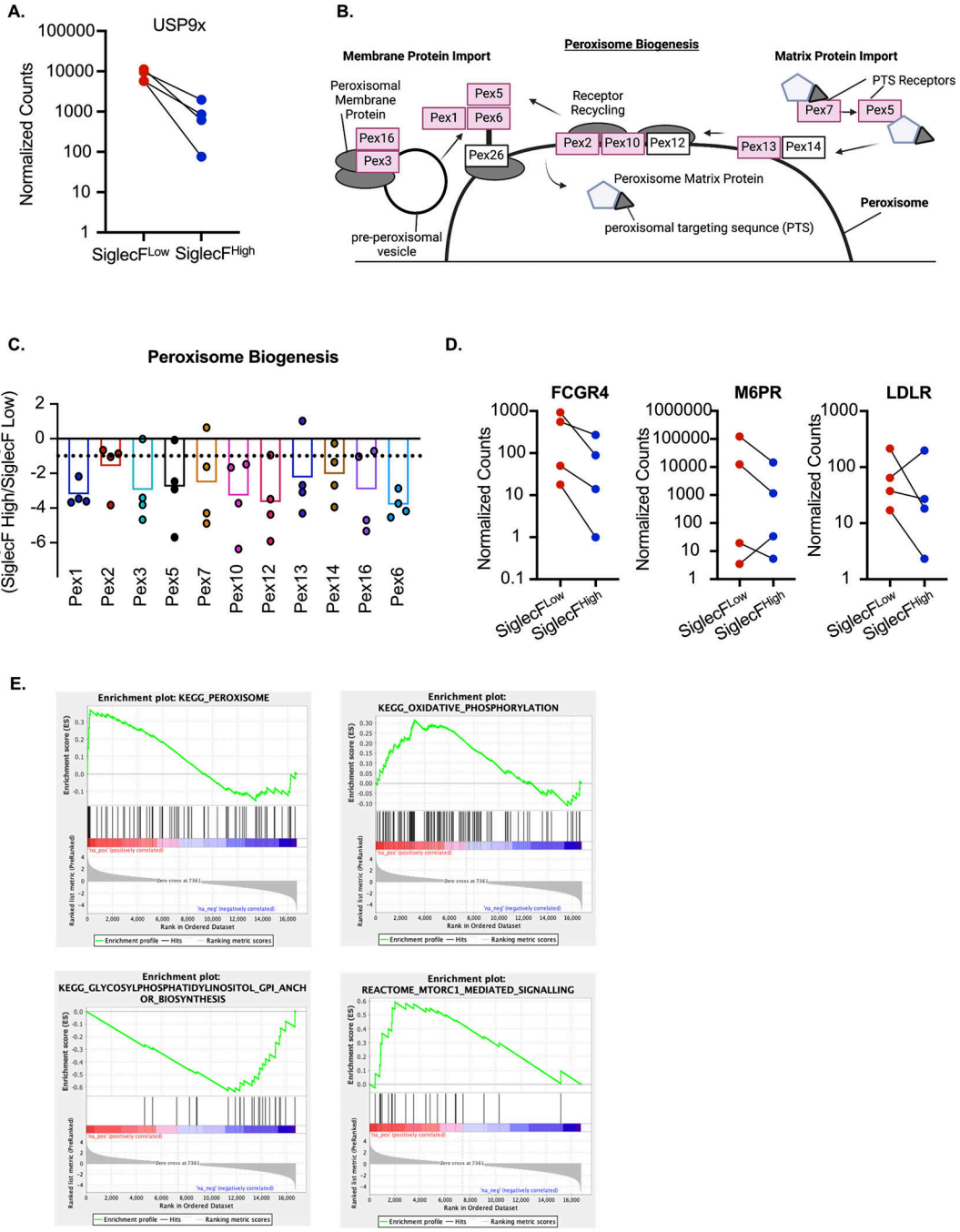

Figure 6. Bioinformatic analysis identifies FLAM metabolic networks as critical regulators of Siglec-F expression.

A) The TGFβ response regulator USP9x was a significant hit in the screen. Shown are the normalized counts for each of the four sgRNAs targeting USP9x in each sorted population. **B)** Using DAVID analysis, peroxisome biogenesis was identified as the most significantly enriched KEGG pathway. Shown is an adaptation of the KEGG peroxisome biogenesis pathway highlighting the 10 peroxisome regulators identified in the screen in red. **C)** The sgRNA distribution and mean log-fold change for each peroxisome regulator identified in

the genetic screen are shown. The dashed line indicates a Log_2 fold change of −1. **D)** DAVID analysis identified surface proteins associated with phagocytosis. Shown are the normalized counts for each of the four sgRNAs targeting the indicated surface protein from each sorted population. **E)** GSEA was used to identify enriched pathways from the entire forward genetic screen. Shown are four leading-edge analysis plots that are representative of this analysis for a subset of enriched pathways. These pathways including the peroxisome, oxidative phosphorylation, GPI anchor biosynthesis and mTORC1 signaling.

Key Resources Table

Reagent	Product number	Manufacturer	Location
RBC lysis buffer for mouse	J62150	Alfa Aesar	Waltham, MA \\
High Capacity RNA to cDNA RT Kit	4387406	Applied Biosystems	Waltham, MA\\
Accutase	561527	BD Biosciences	Franklin Lakes, NJ \\
APC anti-mouse CD11c Antibody	11730	Biolegend	San Diego, CA \\
APC/Cyanine7 anti-mouse CD14 Antibody	123317	Biolegend	San Diego, CA \\
Mouse FC Block	101319	Biolegend	San Diego, CA \\
PE anti-mouse CD170 (Siglec-F) Antibody	155505	Biolegend	San Diego, CA \\
Circular coverslips	72196–12	Electron Microscopy Sciences	Hatfield, PA \\
DMEM	11965092	Gibco	Waltham, MA \\
RPMI	21875034	Gibco	Grand Island, NY \\
Fetal Bovine Serum	100099141	Gibco	Waltham, MA \\
Phenol red-free RPMI 1640	11835030	Gibco	Waltham, MA \\
0.5 M EDTA	15575–038	Invitrogen	Grand Island, NY \\
Penicillin-Streptomycin	15140122	Invitrogen	Carlsbad, CA \\
Bovine Serum Albumin	A3912–100G	Millipore Sigma	Burlington, MA\\
Dulbecco's Phosphate Buffered Saline	D8537	Millipore Sigma	Burlington, MA \\
Lipopolysaccharide from Salmonella Enterica	L6143	Millipore Sigma	Burlington, MA \\
Nigericin	N7143	Millipore Sigma	Burlington, MA \\
Triton X-100	T8787	Millipore Sigma	Burlington, MA \\
hTGFbeta	100–21	Peprotech	Cranbury, NJ \\
mGM-CSF	315–03	Peprotech	Cranbury, NJ \\
RNeasy Isolation Kit	74106	Qiagen	Germantown, MD \\
RNEasy Mini Kit	74104	Qiagen	Germantown, MD \\
Fetal Bovine Serum	S11150H	R\&D Systems	Minneapolis, MN \\
IL-1α DuoSet ELISA	DY400	R\&D Systems	Minneapolis, MN \\
IL-1β DuoSet ELISA	DY401	R\&D Systems	Minneapolis, MN \\
Mouse GM-CSF DuoSet ELISA	DY415	R\&D Systems	Minneapolis, MN \\
Mouse IL-1 alpha/IL-1F1 DuoSet ELISA	DY400	R\&D Systems	Minneapolis, MN \\
Mouse IL-1 beta/IL-1F2 Duoset ELISA	DY401	R\&D Systems	Minneapolis, MN \\
Mouse IL-10 DuoSet ELISA	DY417	R\&D Systems	Minneapolis, MN \\
LysoTracker Red	L7528	Thermo Fisher	Carlsbad, CA \\
SYTOX Green	S7020	Thermo Fisher	Carlsbad, CA \\
TaqMan Gene Expression Master Mix	4304437	Thermo Fisher	Carlsbad, CA \\
High-capacity cDNA Reverse Transcription Kit	4368814	Thermo Fisher Scientific	Waltham, MA \\
Mouse FAM-MGB Taqman probes	4331182	Thermo Fisher Scientific	Waltham, MA \\
Pierce™ TMB Substrate Kit	34021	Thermo Fisher Scientific	Waltham, MA \\
FluoroBrite DMEM	A1896701	Thermo Fisher Scientific	Carlsbad, CA \\
Silica	Min-U-Sil-5	U.S. Silica	Pittsburgh, PA \\
40μm Cell Strainer	229482	Celltreat	Pepperell, MA \\
Tris	T-400	GoldBio	St. Louis, MO \\

Reagent	Product number	Manufacturer	Location
Sodium dodecyl sulfate	L3771	Millipore Sigma	Burlington, MA \\
Proteinase K	EO0491	Thermo Fisher	Carlsbad, CA \\
RNase A, DNase and protease-free	EN0531	Thermo Fisher	Carlsbad, CA \\
Tris-EDTA buffer solution	T9285	Millipore Sigma	Burlington, MA \\
Ammonium acetate	A16343	Alfa Aesar	Waltham, MA \\